energies

MDPI

Article

The Trade-Off between Combustion and Partial Oxidation during Chemical Looping Conversion of Methane

Francesco Miccio [1,*], Mauro Mazzocchi [1], Mattia Boscherini [2], Alba Storione [2], Matteo Minelli [2] and Ferruccio Doghieri [2]

[1] Institute of Science, Technology and Sustainability for Ceramics (ISSMC), National Research Council of Italy, Via Granarolo 64, 48018 Faenza, Italy; issmc@issmc.cnr.it

[2] Department of Civil, Chemical, Environmental and Materials Engineering (DICAM), Alma Mater Studiorum, University of Bologna, Via U. Terracini 28, 40131 Bologna, Italy; mattia.boscherini3@unibo.it (M.B.); alba.storione2@unibo.it (A.S.); matteo.minelli@unibo.it (M.M.); ferruccio.doghieri@unibo.it (F.D.)

* Correspondence: francesco.miccio@cnr.it

Abstract: The chemical looping reforming and combustion of methane have attracted increasing interest as processes for clean energy and syngas production, with potential to reduce carbon dioxide emissions. Previous literature on the development of oxygen carriers evidenced the effects that oxygen availability exerts on the selectivity of the oxidation reaction. In the present paper, we evaluate the performance of chromite sand (Chro), cerium dioxide (CeO_2), and mixed cerium–copper oxide (Ce–Cu) as oxygen carriers for either reforming or combustion according to their oxygen availability. The oxides are tested in 2 to 5 min reduction intervals in a CH_4/N_2 mixture (5, 10 and 20% vol.) followed by regeneration in O_2/N_2 (3, 5, or 21% vol.), with redox cycles conducted either at 850 °C or 950 °C. The obtained rank of selectivity towards complete CH_4 combustion is Ce–Cu > CeO_2 > Chro. Another relevant finding is the role of the degree of carrier conversion in promoting partial or total oxidation. In particular, the selectivity towards CO_2 markedly decreases at increasing carrier conversion, disclosing new strategies for process design and optimization by controlling the carrier conversion degree.

Keywords: chemical looping; combustion; reforming; methane; oxygen carrier

Citation: Miccio, F.; Mazzocchi, M.; Boscherini, M.; Storione, A.; Minelli, M.; Doghieri, F. The Trade-Off between Combustion and Partial Oxidation during Chemical Looping Conversion of Methane. *Energies* **2024**, *17*, 2764. https://doi.org/10.3390/en17112764

Academic Editor: Alberto Pettinau

Received: 19 May 2024
Revised: 31 May 2024
Accepted: 3 June 2024
Published: 5 June 2024

1. Introduction

Chemical looping combustion is an emerging technology allowing for the inherent separation of CO_2 in flue gases [1,2].

It is accomplished by using a suitable oxygen carrier, usually a metal oxide with multiple oxidation states (e.g., FeO_x, MnO_x, NiO_x), and it has the important advantage of limiting NO_x formation thanks to the flameless behavior and well controlled process temperature [3]. Chemical looping can also be effectively used for the reforming and partial oxidation of methane, with high selectivity toward H_2 and CO depending on the nature of the carrier [4]. Cu and Ni oxides generally favor complete oxidation, while cerium oxide is more suitable for partial oxidation to CO. In addition to selectivity, other crucial issues to consider for oxide selection in chemical looping operation are coke deposition and carrier lifetime, in particular, for fluidized bed systems, where attrition phenomena are more relevant [2]. Furthermore, the safety and disposal of the spent carrier are also fundamental aspects that need to be explored. In this respect, the use of Ni compounds is decreasing due to concerns about their toxicity [5].

The trade-off between combustion and partial oxidation is somehow connected to the prompt availability of oxygen-rich sites in the microstructure of the carrier. In the case of cerium dioxide, for example, it has been repeatedly observed that while the production of carbon monoxide is overall favored compared to combustion, carbon dioxide can be nonetheless formed at the start of the reaction due to the high availability of surface

oxygen species [6,7]. The availability of surface oxygen, related to the energy barrier for oxygen vacancy formation, the amount of total oxygen available for exchange (oxygen carrying capacity), the morphology and the surface chemistry, particularly oxygen vacancy concentration, all greatly affect the selectivity of oxidation [8]. For example, it has been suggested that the mechanism of methane oxidation on cerium dioxide changes as surface oxygen is depleted, with the activation of methane occurring preferentially on oxygen anions at the start of reaction, while on more reduced surfaces activation occurs also on oxygen vacancy sites [9]. Oxygen vacancies have also been observed to play a critical role in determining selectivity for reforming over combustion for iron oxygen carriers [10], with increased vacancy concentration favoring the partial oxidation of methane and lowering the energy barrier for C–H bond cleavage. In the present paper, we further investigate this shift in selectivity, which needs to be carefully evaluated to properly design the chemical looping process.

Natural chromite sand, made of a mixture of chromium and iron oxide mixed with other species such as alumina, silica, and others, is commonly used in metallurgy as foundry sand and as a source of chromium [11,12]. It has been previously investigated, as a catalyst, for use in fluidized bed combustion for CO abatement providing limited advantages [13], whilst copper-modified chromite proved more effective [14]. Its potential application as an oxygen carrier has, to the author's knowledge, so far not been investigated at depth in the literature. However, due to its inclusion of high concentrations of oxidation active iron oxide species (especially in low-grade chromite sands) and its high melting point, these materials may deserve further investigation. Copper oxide is a well-known catalyst for low-temperature combustion as well as for the decomposition of methane [15], but it is not commonly used for reforming processes. The use of CeO_2 for reforming processes has been investigated via several aspects, in particular the redox kinetics and carbon deposition at different temperatures and residence times [7,16,17]. Chemical looping combustion with CuO or CeO_2 has also been tested in fluidized bed apparatus [18–20], providing good results in terms of the material's lifetime, mechanical resistance, and regeneration efficiency.

The aim of the present research is to understand the potential use and the chemical behavior of different natural and synthetic oxygen carriers under changing operating conditions, moving from chemical looping combustion to partial methane oxidation. The influence of equivalence factor, temperature and conversion time is reported and discussed to provide further insights into the design of the process and the materials.

2. Materials and Methods

2.1. Materials

Three types of oxygen carriers have been selected: natural chromite sand (Cromitec 400, hereafter defined Chro), CeO_2 and CeO_2/CuO (samples named Ce–Cu) granules.

Commercial powders of CeO_2 (PIKEM, Wilnecote, UK) and CuO (Merck, Darmstadt, Germany) have been uniaxially pressed around 90 MPa, obtaining 20 mm diameter pellets subsequently crushed and sieved to 0.60–0.84 mm and thermally treated for 20 min in air at 900 °C.

For all the prepared materials O_2 capacity was computed based on reducible species content. The main properties of the carriers are reported in Table 1.

Cerium–copper carrier exhibits the highest O_2 capacity value while chromite has the lowest, the oxygen capacity being related to FeO alone; therefore, this excludes the possibility that Cr_2O_3 can be reduced at the process temperature.

Samples of the carriers have been characterized by electronic microscopy FE-SEM (Zeiss SIGMA, Carl Zeiss Microscopy GmbH, Jena, Germany, D) and X-ray powder diffractometry (XRD) using a Bruker D8 Advance (Bruker–Karlsruhe, Karlsruhe, Germany, D) diffractometer.

Table 1. Properties of oxygen carriers.

	Chro	CeO_2	Ce–Cu
Size (mm)	0.20–0.40	0.60–0.84	0.60–0.84
Density (kg/m^3)	4170	7220	6930
O_2 capacity (mmol/g)	0.90	1.45	2.98
Major phases			
CeO_2, wt. %	-	>99	68
CuO, wt. %	-	-	32
Cr_2O_3, wt. %	47	-	-
FeO, wt. %	26	-	-
Al_2O_3, wt. %	15	-	-
MgO, wt. %	10	-	-
SiO_2, wt. %	1	-	-

2.2. Experimental Apparatus

The schematic of the experimental rig used for chemical looping tests is shown in Figure 1. The reactor is a 10 mm ID quartz tube equipped with a ceramic distributor in the bottom. The reactor is installed inside an electric furnace (Carbolite 1200, Carbolite LTD, Hope Valley, UK). Bronkhorst mass-flowmeters are used to supply gas streams from compressed gas bottles (O_2, N_2, CH_4). A Pollutek GAS-3100P continuous gas analyzer (Pollutek Gas Analysis, Lubbeek, Belgium) has been employed for O_2, CO, CO_2, CH_4 and H_2 detection.

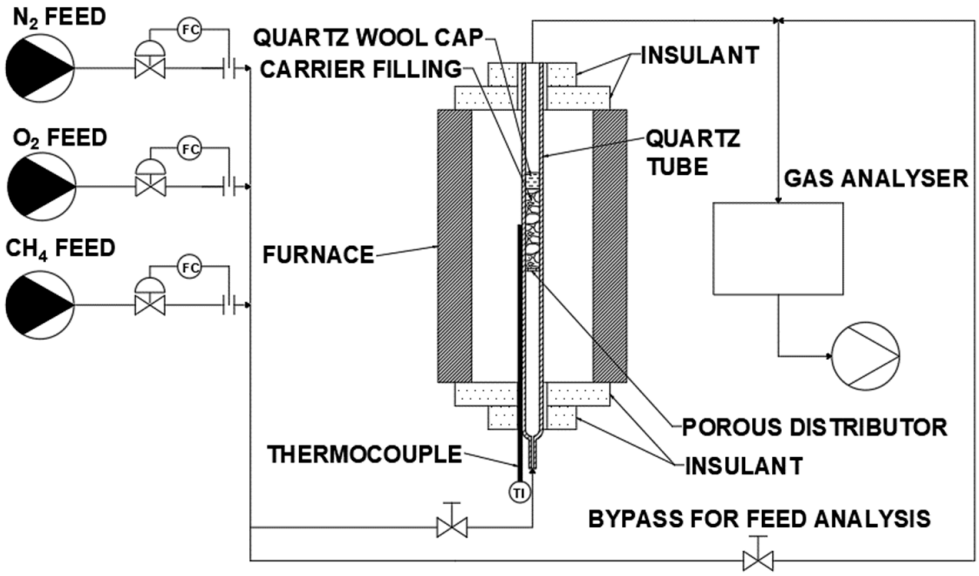

Figure 1. Schematic of the experimental apparatus. Flowrate Controller (FC) indicates the flowmeters. Temperature Indicator (TI) indicates the thermocouple.

In a typical experiment, a mass of 14 to 16 g of oxygen carrier is loaded in the reactor to ensure the same bed volume for the three oxygen carriers (≈5 cm^3), with a layer of ceramic wool on the top of the bed to limit fluidization and avoid the entrainment of particles outside the reactor. The residence time of the gas stream in the fixed bed was lower than 0.1 s. For the half cycle of reduction, streams of 1 NL/min of CH_4 at 5, 10 and 20 vol.% in N_2 were selected to study the effect of methane concentration on reaction selectivity, while for carrier regeneration, streams of O_2 at 3, 5, or 21 vol.% in N_2 at a total 1 NL/min flow rate were evaluated. The main factor in the choice of oxygen concentration during regeneration was the necessity to avoid overheating triggered by the exothermic reaction without loss in regeneration efficiency.

Reduction experiments were carried out by varying the time between 2 and 10 min, while for regeneration the reactor was kept on stream until a breakthrough in the inlet oxygen molar fraction was obtained.

2.3. Data Elaboration

The CH_4 conversion, ξ_{CH_4}, is evaluated by the integration of the difference between the inlet and outlet methane flow rate divided by the methane fed during the reduction step of length t_c = 2, 5 or 10 min (Equation (1)). The outlet molar flow rate is calculated using N_2 balance as a reference.

$$\xi_{CH_4} = \int (q_{in} \times y_{CH_4,in} - q_{out} \times y_{CH_4,out})dt/(q_{in} \times y_{CH_4,in} \times t_c) \quad (1)$$

The CO and CO_2 selectivity (η_{CO}, η_{CO_2}) are computed (Equations (2) and (3)) based on the converted CH_4 by integration of their molar fraction profiles,

$$\eta_{CO} = \int (q_{out} \times y_{CO,out})dt/(q_{in} \times y_{CH_4,in} \times t_r) \quad (2)$$

$$\eta_{CO_2} = \int (q_{out} \times y_{CO_2,out})dt/(q_{in} \times y_{CH_4,in} \times t_r) \quad (3)$$

Carbon deposition is calculated from carbon balance by considering the amount of CO and CO_2 released during the regeneration stage, also calculated by integrating the molar fraction profile. Carbon selectivity can therefore be obtained as

$$\eta_C = \int (q_{out} \times y_{CO,out} + q_{out} \times y_{CO_2,out})dt/(q_{in} \times y_{CH_4,in} \times t_c) \quad (4)$$

The equivalence factor of a single run corresponds to

$$e = n_{O_2\ av,i}/n_{O_2\ stoich,\ CH_4} \quad (5)$$

where $n_{O_2\ stoich,\ CH_4}$ indicates the moles of oxygen necessary for stoichiometric total combustion of the total fed methane, while $n_{O_2\ av,i}$ is the total amount of oxygen which can be released from the carrier i.

$$n_{O_2\ stoich,\ CH_4} = 2(q_{in} \times y_{CH_4,in} \times t_c) \quad (6)$$

The reactions considered for carrier reduction are

$$2CeO_2 \rightarrow Ce_2O_3 + 1/2O_2 \quad (R1)$$

$$Fe_2O_3 \rightarrow 2FeO + 1/2O_2 \quad (R2)$$

$$CuO \rightarrow Cu + 1/2O_2 \quad (R3)$$

Therefore, for cerium dioxide, the amount of available oxygen was calculated considering complete reduction to Ce_2O_3:

$$n_{O_2\ av,\ CeO_2} = 1/4(m_{CeO_2}/M_{CeO_2}) \quad (7)$$

For chromite, the amount of oxygen was calculated considering the FeO content of chromite only (Table 1), the reduction of the other oxides contained in chromite being thermodynamically hindered at the investigated temperature. The maximum releasable O_2 content derives from converting FeO to Fe_2O_3 and then reducing it back to FeO (Equation (8)), ω_i being the generic mass fraction of the component i. The reduction of FeO to metallic Fe was excluded,

$$n_{O_2\ av,\ Chro} = 1/4(m_{Chro} \times \omega_{FeO})/M_{FeO} \quad (8)$$

While the thermodynamic formation of completely reduced Fe would be feasible, metallic iron was not observed in the XRD patterns of reduced samples. Similarly, Leion et al. also excluded the total reduction of iron when discussing the use of ilmenite as an oxygen carrier [21].

For the Ce–Cu carrier, both reactions R1 and R3 were considered,

$$n_{O_2\ av,\ Ce\text{-}Cu} = 1/4(m_{Ce\text{-}Cu} \times \omega_{CeO_2})/M_{CeO_2} + 1/4(m_{Ce\text{-}Cu} \times \omega_{CuO})/M_{CuO} \quad (9)$$

The oxygen capacity (Table 1), reported as mmol of O_2 per gram, is also used to evaluate the conversion degree of the carrier, $\xi_{carrier}$, obtained by evaluating the total oxygen released during the reduction step through oxygen balance for CO, CO_2, O_2 and H_2O species, H_2O production being estimated via hydrogen balance.

$$\xi_{carrier} = \int \{q_{out} \times [0.5 \times y_{CO,\ out} + y_{CO_2,out} + y_{O_2,out}] + 0.5[2 \times q_{in} \times y_{CH_4,in} - q_{out} \times (2 \times y_{CH_4,out} - y_{H_2,out})]\}dt/n_{O_2,av,carrier} \quad (10)$$

where "carrier" indicates Chro, CeO_2, or Ce–Cu.

Experimental errors are mainly caused by the intrinsic transient character of the looping operation and are estimated in ±10% of the reported data.

3. Results

3.1. Reaction Test Results

Figure 2 shows the volumetric fraction profiles of CH_4, CO, CO_2, H_2 and O_2 for both oxidation (t = 1 ÷ 3 min) and regeneration (t = 4 ÷ 9 min) on the Chro carrier for a 2′ reduction step in 10% methane followed by 6′ regeneration in 3% O_2. A 1′ flushing with N_2 was performed in the passage from oxidation to regeneration and vice versa. It is clearly visible how the volume fractions change as reaction proceeds, with CO_2 production decreasing during the reduction step, whilst the H_2 and CO volume fractions increase. Similar profiles are also observed over CeO_2, while for the Ce–Cu carrier, CO and H_2 production were found to be almost completely absent, even for longer reduction steps. Considering an equal mass of carriers, the Ce–Cu carrier theoretically offers the highest oxygen availability compared to the other two tested (see Table 1). Also, the Ce–Cu carrier is the only one that shows the release of gaseous oxygen due to thermal dissociation at the investigated temperature, thus providing oxygen in a larger amount for reaction with methane.

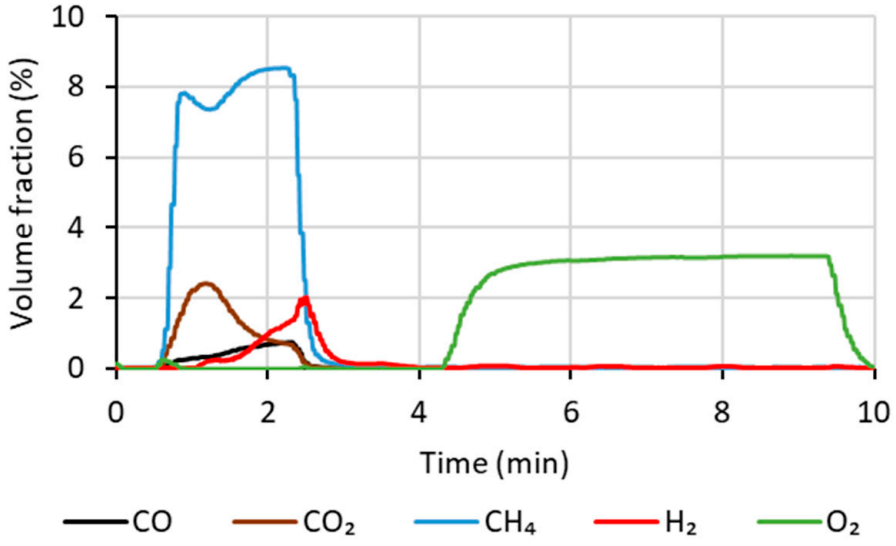

Figure 2. Volume fraction profiles of CH_4, CO, CO_2, H_2 and O_2 during a test at 950° (Chro, y_{CH_4} = 0.10, Y_{O2} = 0.03).

Figure 3 shows the comparison among Chro, CeO_2 and Ce–Cu carriers in terms of CH_4 conversion for tests carried out at 850 and 950 °C with reduction time of 2 or 5 min. It is clear that, in terms of maximum methane conversion, the rank of the carrier is Ce–Cu > CeO_2 > Chro, as a consequence of the difference in O_2 capacity and availability. Oxygen is the most widely available in the Ce–Cu carrier, both in terms of the quantity of available oxygen (Table 1) and of the easiness of oxygen release, as it is the only investigated material that releases gaseous oxygen at the investigated reaction temperature. Therefore, it is not surprising that methane conversion is greatest for this material, as the combustion reaction is not strictly surface-mediated, but can also involve fully gaseous species. It is worth noting that this Chemical Looping Oxygen Uncoupling (CLOU) mechanism [22] is also likely responsible for the similar values of ξ_{CH_4} at 850 and 950 °C for Ce–Cu, owing to the capability of this carrier to make available gaseous molecular O_2 imposing a less strict limit on process kinetics compared to the strictly surface-mediated oxidation on the other carriers, with the presence of metallic Cu further favoring the reaction by providing active sites for methane C–H bond cleavage.

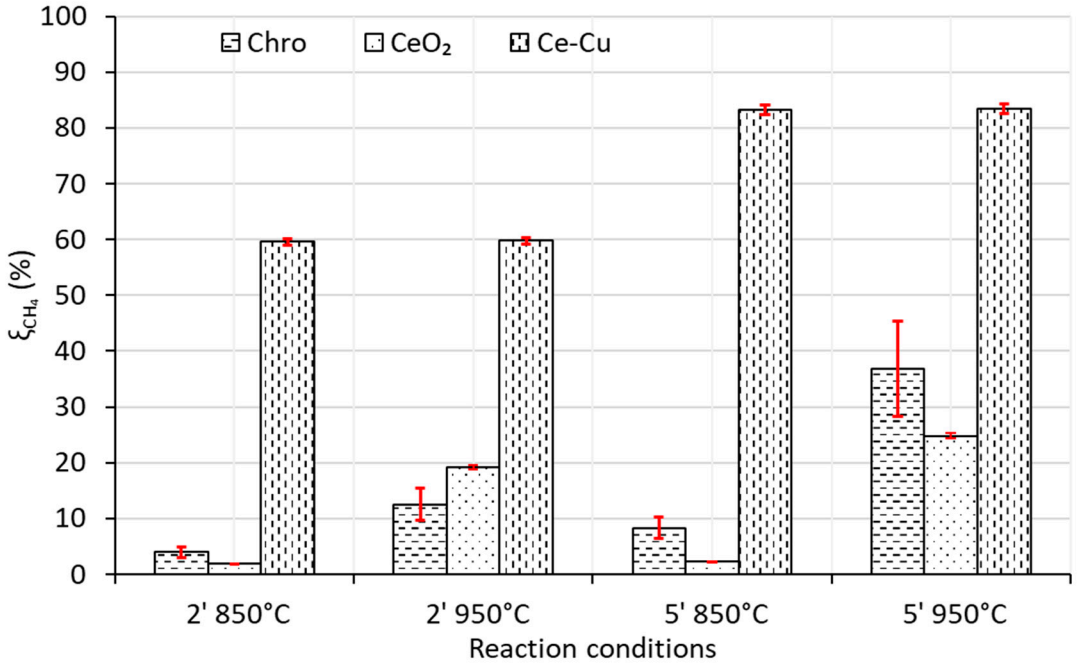

Figure 3. Average CH_4 conversion in Chro, CeO_2 and Ce–Cu carriers at 850 and 950 °C (y_{CH_4} = 0.10); the error bars reported in red in the plot indicate the standard deviation in triplicate tests.

On the contrary, the very low values of ξ_{CH_4} obtained for Chro and CeO_2 carriers at 850 °C moved the investigation preferably to the temperature of 950 °C. Furthermore, Chro carrier exhibited greater instability in performance, particularly after undergoing cycles at 950 °C. After undergoing reaction at 950 °C, the material appeared more effective even at a lower temperature: the observed average ξ_{CH_4} for 2 min partial oxidation steps at 850 °C was 1.7 ± 0.2% for fresh material, while it increased to 7.4 ± 0.4% after the material underwent reaction at a higher temperature. It is likely that the material undergoes structural changes during operation at higher temperatures. Once extracted from the reactor, Chro carrier was found to be partly sintered, and this could be the reason for the differences in performance.

Table 2 reports the selectivity and yield data for Chro, CeO_2 and Ce–Cu at 950 °C and y_{CH_4} = 0.10. The equivalence factor changes largely due to the difference in oxygen capacity of the three carriers. The greater availability of oxygen in Ce–Cu clearly appears, resulting in conversion up to 0.83 and the total combustion of methane regardless of the

total reduction time. The catalytic activity was retained over repeated cycles (>10) of reduction and oxidation for all samples.

Table 2. CH_4 conversion, CO selectivity and CO_2 selectivity for Chro, CeO_2 and Ce–Cu carriers (y_{CH_4} = 0.10, 950 °C).

	Time, min	e	ξ_{CH_4}	η_{CO}	η_{CO_2}
Chro	2	0.81	0.13	0.12	0,29
	5	0.32	0.37	0.45	0,00
CeO_2	2	1.25	0.19	0.24	0.78
	5	0.50	0.25	0.58	0.54
Ce–Cu	2	2.48	0.60	0.00	1.00
	5	0.99	0.83	0.00	1.00

For Chro and cerium dioxide, selectivity and conversion change throughout the reaction.

Figure 4 shows CH_4 conversion, and CO and CO_2 selectivity, at different CH_4 concentrations, as well as reduction time over CeO_2 carrier. The trends in the changes of these variables are mutually consistent: ξ_{CH_4} decreases as the mole fraction of CH_4 increases, corresponding to a lower equivalence factor in the whole test. Selectivity towards partial oxidation also increases with a longer reduction time.

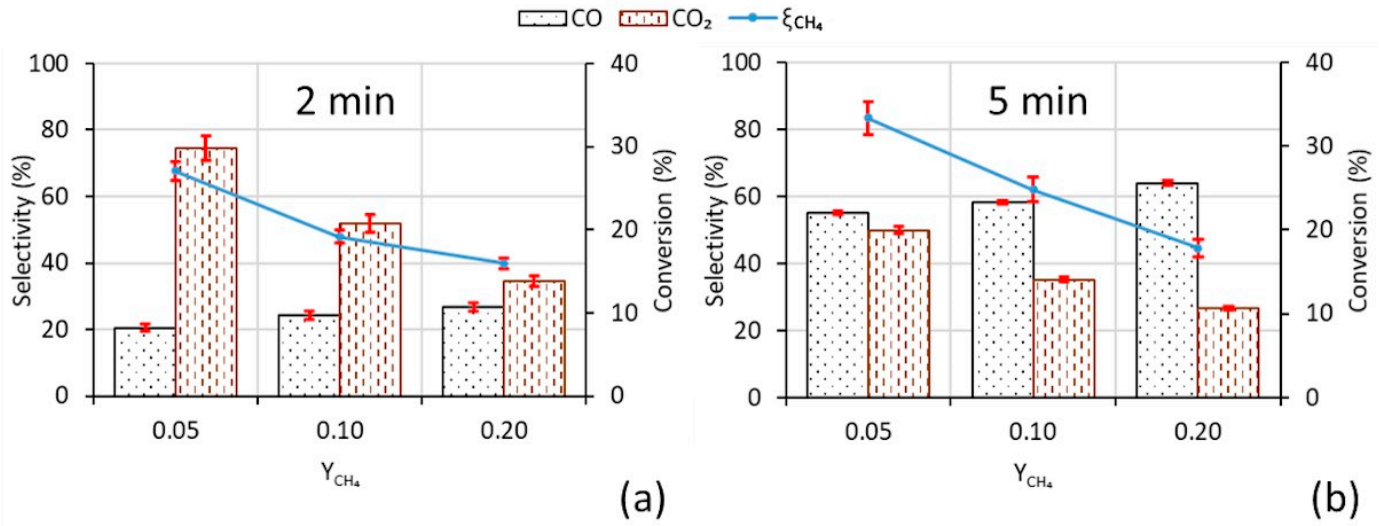

Figure 4. CH_4 conversion, CO selectivity and CO_2 selectivity over CeO_2 carrier at 950 °C, Y_{CH_4} = 0.05, 0.10 and 0.20: (**a**) reduction time 2 min, (**b**) reduction time 5 min; the error bars in the plot indicate the standard deviation in triplicate tests; the error bars reported in red in the plot indicate the standard deviation in triplicate tests.

The selectivities of CO and CO_2 clearly exhibit opposite trends when increasing the mole fraction of CH_4 for both reduction times. Therefore, the conditions required to achieve total combustion, over CeO_2, are those corresponding to a short reduction time and low y_{CH_4}, i.e., a higher equivalence factor.

Experimental data, for all carriers, have also been evaluated to allow for consideration of carbon deposition. Coke formation was appreciable only for experiments carried out at 950 °C, where the presence of carbon lowered the selectivity towards CO_2 and CO. Table 3 reports the carbon selectivity, η_C, for these tests, which is always below 10%, with the exception of the test with Chro at y_{CH_4} = 0.10 and t = 5′ (η_C = 11.9%), which was affected by a partial agglomeration of the fixed-bed particles. The accumulated carbon was readily converted during carrier regeneration, without causing apparent problems to carrier regeneration.

Table 3. Carbon (coke) selectivity (%) in Chro, CeO_2 and Ce–Cu at different y_{CH_4} and oxidation times (T = 950 °C).

y_{CH_4}	0.05	0.05	0.10	0.10	0.20	0.20
Time, min	**2**	**5**	**2**	**5**	**2**	**5**
Chro	3.5	0.7	1.3	11.9	-	-
CeO_2	7.7	2.4	4.4	1.1	1.0	0.7
Ce–Cu	0.8	0.1	0.5	1.4	4.6	2.6

Mean standard deviation ±0.3.

Figure 5 displays the instantaneous selectivity towards CO and CO_2 for tests carried out with CeO_2 carrier at 950 °C and increasing y_{CH_4}. The reported behavior is consistent with the changes in operating conditions and the transient character of the test. CO_2 selectivity was the highest at the initial time, i.e., at maximum equivalent factor ($e \rightarrow +\infty$), and declined with decreasing e, corresponding to the progressive depletion of oxygen sites in the carrier. The increase in the mole fraction of CH_4 leads to a shift in the CO_2 curves towards lower values due to the lower equivalence factor and the lower availability of oxygen. Congruently, the selectivity behavior of CO is perfectly symmetrical with that of CO_2.

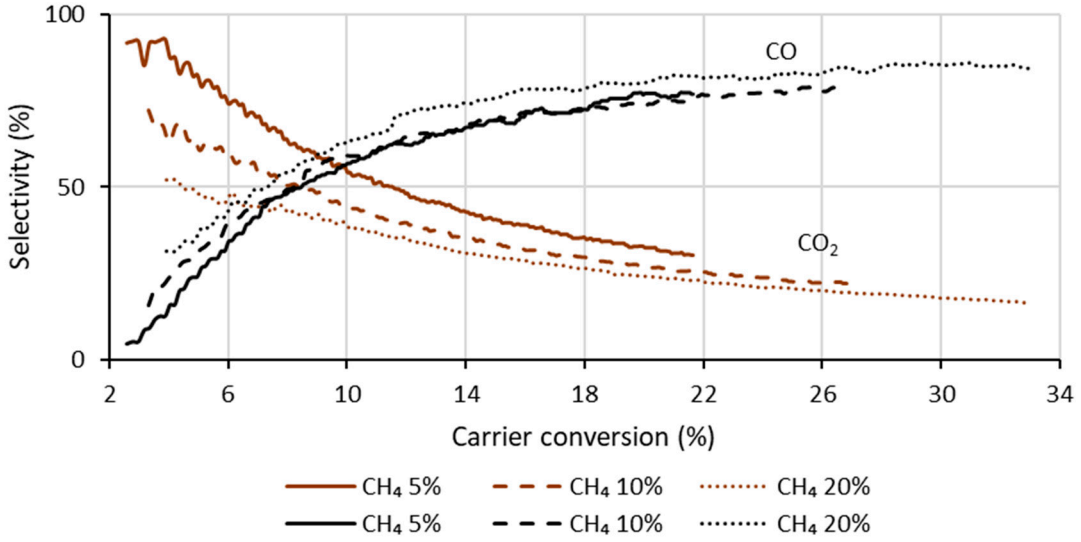

Figure 5. Instantaneous CO and CO_2 selectivity in CeO_2 carrier at Y_{CH_4} = 0.05, 0.10 and 0.20 as a function of carrier conversion degree (t_c = 5′, T = 950 °C).

3.2. Characterization of the Samples

Oxygen carriers, before and after use in the reactor, have been characterized by SEM and XRD analyses.

Figure 6 displays the SEM images of the granules at different magnifications. Low-magnification images (Figure 6a,b) demonstrate that for the CeO_2 and Ce–Cu carrier, the granules remain almost unchanged before and after use in the reactor. No fine particles were formed during reaction, which is reasonable, as the tests were carried out in a fixed bed without abrasion and rather limited thermal stress. In general, all granules are dense with well-defined external surfaces. Therefore, we have confirmed the good mechanical stability of both synthetic CeO_2 and Ce–Cu carriers. The morphology of Chro carrier granules recalls the cubic-octahedral symmetry of the material with isometric/rounded granules with smooth surfaces and without microstructures, a bit like crystalline faces. Some particle agglomerates are also evident in the case of chromite use (Figure 6b). In this regard, a rather large agglomerate was recovered after unloading the chromite bed, while the other two materials did not present similar problems.

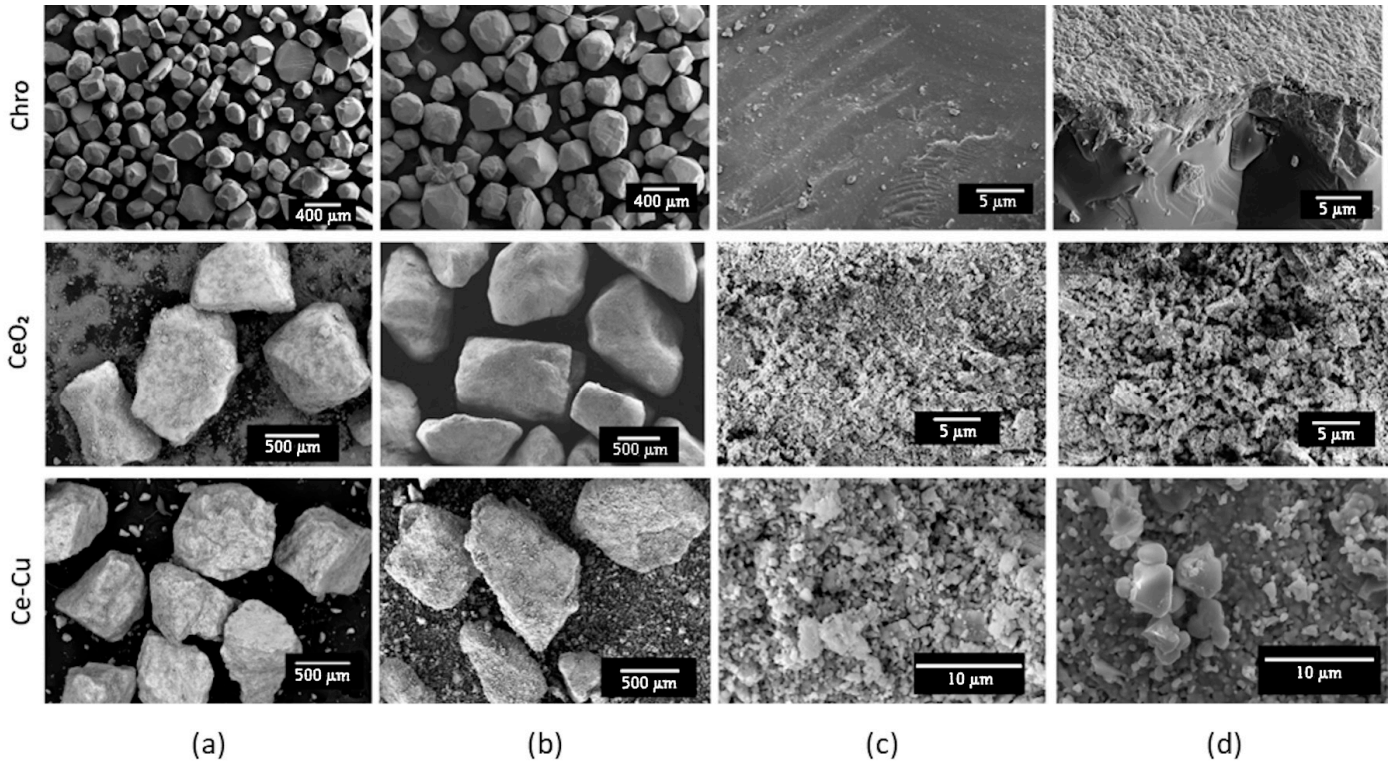

Figure 6. SEM images of Chro, CeO_2 and Ce–Cu granules at 10× (**a**,**b**) and 10,000× (**c**,**d**) magnification before (**a**,**c**) and after (**b**,**d**) utilization in the reactor.

The XRD analysis (Figure 7) proves that before and after the test, the CeO_2 and Ce–Cu samples were very similar, without substantial crystallographic–structural and crystalline difference. Only a certain difference can be seen in terms of crystallite size. The Ce–Cu carrier exhibits some peaks of CuO (pristine oxide) and Cu_2O, as a consequence of the reduction step and incomplete regeneration. Conversely, before and after the test, chromite samples exhibit large differences with clear oxidation phenomena and the presence of Fe_2O_3 peaks in the one subjected to chemical looping. Some spinel structures between Fe and Chro oxides also appear for the used Chro carrier. Also, a higher baseline for chromite is present due to the lower degree of crystallinity of this natural material.

Ceria samples do not exhibit a substantial presence of any additional phases or Cerium oxide with different oxidation states (e.g., Ce_2O_3), and they appear quite pure and composed of a single phase according to XRD analysis. Even after undergoing several reaction steps, the material does not display any relevant change, either from the chemical or structural point of view (e.g., entry or loss of oxygen), with no apparent change in cell parameters. Both the spacing and intensity of reflections are completely coherent before and after treatment. This finding suggests very good stability and regeneration efficiency.

Ce–Cu samples are also very similar before and after reaction, without substantial crystallographic–structural and crystalline difference in the present CeO_2, before and after treatment. The only changes in Ce–Cu carrier are exhibited concerning the copper phase, with some peaks of Cu_2O (cuprite) appearing together with CuO (tenorite, as pristine oxide) peaks in the spent material, as a consequence of the reduction step and incomplete regeneration. Concerning this regeneration process, some traces of the presence of an intermediate oxidative phase, where copper is present with both oxidation numbers as Cu_4O_3 (paramelaconite, where $Cu^{1+}{}_2Cu^{2+}{}_2O_3$), have been found [23]. Even a certain difference could be appreciated in terms of crystallite size before and after treatment.

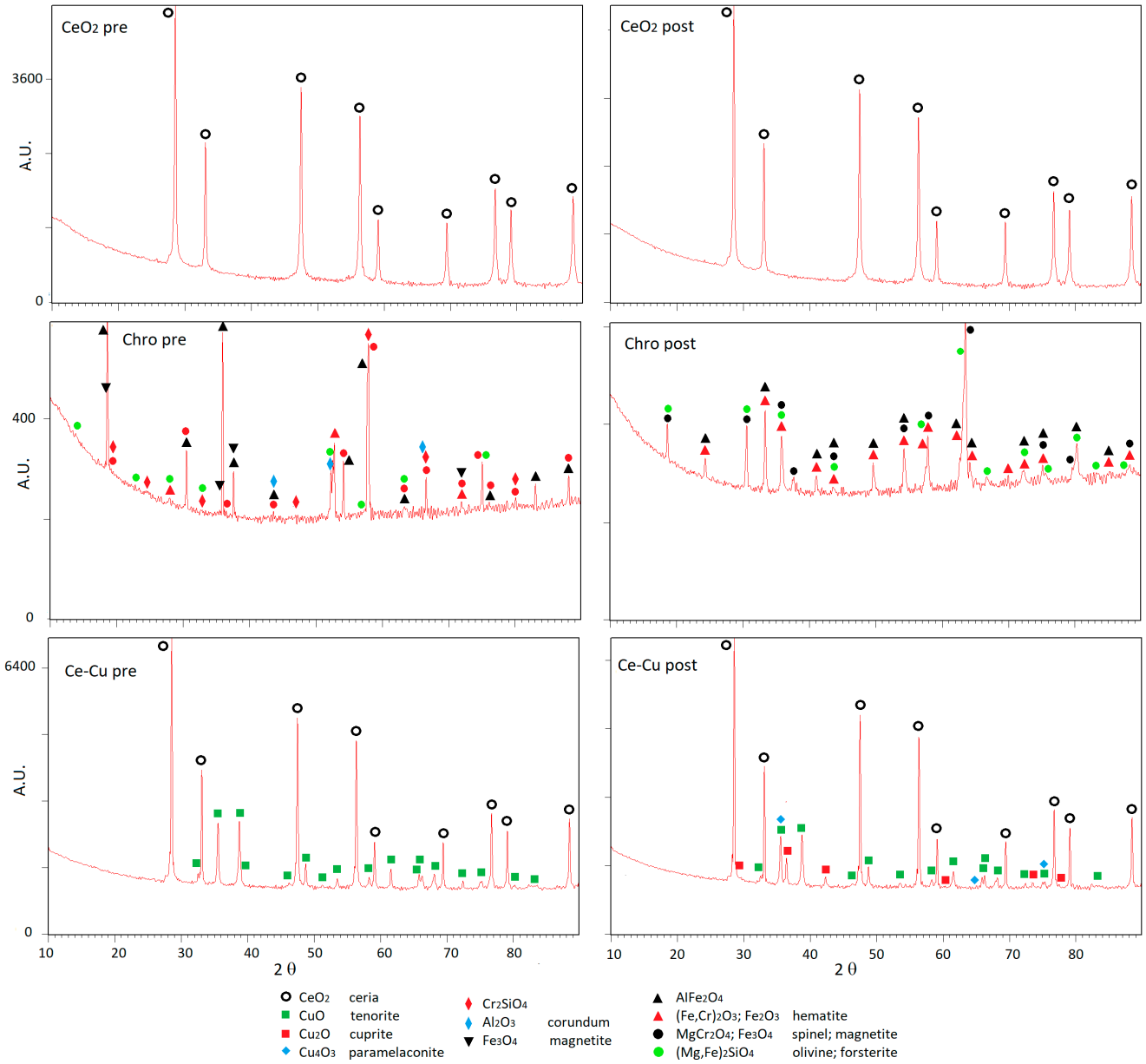

Figure 7. XRD patterns of Chro, CeO_2 and Ce–Cu before and after utilization in the reactor.

The chromite sample comes from mineral natural sand collecting several spinel phases with a complex stoichiometry $(Mg,Fe)(CrAl)_2O_4$, $Fe(Cr,Al)_2O_4$, $AlFe_2O_4$, etc., according to the main elements already found in the chemical analyses. The higher baseline of the patterns is due to a fluorescence effect of XRD in the presence of transition metals (Mn, Co, Ni, Fe, Cr, and others). Only a few traces of accessory residual and refractory mineral phases have been found (e.g., corundum, magnetite, olivine).

4. Discussion

Table 4 provides a comparison of methane conversion and selectivity as the input mole fraction and carrier conversion vary for the three materials investigated. The cells in which there are high values (0.50) of selectivity in CO_2 and CO have been highlighted in dark and light grey, respectively. Despite some inconsistencies due to the limits of the experimental technique, especially regarding short conversion times, it can be noted that the initial phases of reaction ($\xi_{carrier}$ = 0.1) favor the total oxidation of methane with the production of CO_2, while the progress of the carrier conversion ($\xi_{carrier}$ = 0.2) leads to the

partial oxidation and formation of CO. For the values investigated, Ce–Cu always promotes total combustion with the formation of CO_2 and CO present only in traces. This can be attributed to the high O_2 capacity of the carrier, as well as its CLOU behavior due to the release of gaseous oxygen. These results could be linked to the different activities of oxygen sites in the carrier [8], depending on their ease of accessibility.

Table 4. CH_4 conversion, CO and CO_2 selectivity in Chro, CeO_2 and Ce–Cu at different y_{CH_4} values and conversion degrees of the carrier (T = 950 °C).

	y_{CH_4}	0.05	0.05	0.10	0.10	0.20	0.20
	$\xi_{carrier}$	0.10	0.20	0.10	0.20	0.10	0.20
Chro	ξ_{CH_4}	0.18	(-)	0.21	0.14	(-)	(-)
	η_{CO}	0.15	(-)	0.39	0.58	(-)	(-)
	η_{CO_2}	0.85	(-)	0.36	0.35	(-)	(-)
CeO_2	ξ_{CH_4}	0.29	0.28	0.22	0.21	0.17	0.16
	η_{CO}	0.47	0.33	0.59	0.74	0.63	0.80
	η_{CO_2}	0.53	0.77	0.44	0.27	0.39	0.24
Ce–Cu	ξ_{CH_4}	0.73	0.73	0.74	0.74	0.74	0.74
	η_{CO}	0.00	0.00	0.00	0.00	0.00	0.00
	η_{CO_2}	1.00	1.00	1.00	1.00	0.87	0.88

The microstructural analysis showed different behaviors among the three carriers (Figure 6c,d). The granules of CeO_2 retain their surface characteristics well even after exposure to high temperature and redox atmosphere. On the contrary, chromite gives rise to an evident modification of the exposed surface with fractures and the formation of an amorphous layer, while the crystalline structure remains unchanged in the internal core of the granule (Figure 6d). An intermediate behavior occurs for Ce–Cu granules, where some formations of sintered micro-granules are evident (Figure 6d) upon the exposure to high temperature and chemical reaction, probably due to the less refractory character of copper oxide with respect to ceria.

Conversely, before and after the test, chromite samples exhibit large differences with clear oxidation phenomena, with a presence of peaks from neo-formed Fe_2O_3 (particularly lying on the surface of the granules where the oxidation process was more intense) in the one subjected to chemical looping, together with a rearranging of chemical compositions of the phases. Iron oxide phases appear to be segregated on the grain surface. This is consistent with phase diagrams for Fe–Cr–O systems reported in literature [24,25].

The CuO–CeO_2 oxygen carrier displayed the highest oxygen availability, while the chromite carrier showed limited activity towards methane.

Overall, the good selection of reaction step duration is crucial to ensuring the desired process selectivity for all oxygen carriers. Previous literature has suggested that the mechanism of reaction of methane on cerium dioxide changes as the material is reduced [9], and so does the selectivity. Methane was shown to be activated on surface oxygen sites over oxidated cerium dioxide, which are also active in the further oxidation of syngas. As the surface oxygen sites are depleted, methane activation starts occurring on the formed oxygen vacancies, while the lower surface oxygen availability stops the further formation of CO_2 and H_2O. This must be considered when discussing process optimization, and the extent of reduction reached by the carrier can be used to modulate reaction selectivity. Limiting reaction time allows one to reduce coke deposition, but should be accomplished with care, as an overly strict limitation in the reaction step duration can cause a noticeable overall loss in selectivity towards partial oxidation.

In the case of cerium dioxide, the present paper clearly displays the presence of a lower threshold in the extent of carrier conversion that needs to be surpassed if one is to observe a significant prevalence of partial oxidation when compared to complete combustion.

A carrier conversion lower than 10% (Figure 5) in the observed reaction conditions leads to a very high influence of total combustion on process yield. The previous literature on chemical looping over cerium dioxide showed the need for short reaction cycles to avoid excessive carbon deposition [26,27], but this tradeoff between complete and partial oxidation also needs to be addressed when selecting cycle length.

Chromite also displayed a similar behavior to CeO_2 carrier, with a first phase of reaction where complete oxidation is favored followed by a second step with prevalent syngas formation. In this case, the first phase of complete combustion is most likely attributed to the reduction of surface Fe_2O_3 to Fe_3O_4, with the further reduction to FeO being responsible for the generation of syngas, as previously reported in the literature for iron-based oxygen carriers [28]. In general, chromite sand displayed low activity and yields for both chemical looping reforming and combustion, despite its relevant content (26%) of iron species. While iron species demonstrated activity related to methane oxidation, as shown by the XRD patterns, chromium species were shown to not be active in the experimental conditions investigated, and the material displayed significant aggregation and carbon deposition during reduction, leading to an overall unsatisfying performance of the material.

Finally, in the case of the Ce–Cu process, step duration showed no effect on the selectivity towards either complete or partial oxidation for these short reaction times, as oxygen uncoupling favored complete combustion independently of the extent of carrier reduction. The Ce–Cu carrier thus appears to be unsuited for reforming, but shows excellent performance for combustion. For the Ce–Cu carrier, the selection of an ideal reduction step duration would thus mostly be determined by the rate of carbon deposition compared to the rate of oxidation as carrier conversion increases. Previously, Saddiq et al. investigated the kinetics for the oxidation of liquefied petroleum gas (propane/butane mixture) on 10% CuO/CeO_2 powder at 800 °C, and observed that a first-order kinetic model best described the reforming reaction, thanks to the high availability of oxygen, while a shrinking core model best described the reaction rate of pellets of the same material due to reduced oxygen release [29]. Nonetheless, high oxygen release was observed in both cases. He et al. also investigated the use of a 50/50 wt. % CuO/CeO_2 oxygen carrier for methane reforming [30]. They observed an almost complete selectivity towards partial oxidation above 850 °C, coupled with a very high carbon deposition, but this is not consistent with our observed results. In our experiments, the Cu–Ce oxygen carrier was almost completely selective towards complete oxidation both at 850 °C and 950 °C, and carbon deposition became relevant only for the longer-running tests at higher methane concentration. This discrepancy in results could be partly explained by the lower methane concentration and shorter reaction time used in our experiments compared to their results. The high selectivity towards complete combustion observed for our results can also be related to the preparation method employed for the Ce–Cu carrier. He et al. [30] prepared their sample through the co-precipitation method, which may allow a more intimate mixing of the two phases, allowing for cerium dioxide to play a major role in determining process selectivity. Our low carbon deposition results are closer to the observations made by Elgarni et al. [31], who also observed limited carbon deposition for CeO_2-supported CuO. Both Elgarni et al. [31] and Tijani et al. [32] observed a reduction in overall oxygen exchange capacity for CeO_2-supported Cu carriers when increasing the operation temperature above 900 °C, which would coincide with an increase in carbon deposition, but this is not immediately evident in our experimental results, as only limited aggregation was observed in our case for the Ce–Cu carrier.

5. Conclusions

The chemical looping conversion of methane was investigated in a lab-scale fixed-bed reactor. Three oxygen carriers with different oxygen capacities, one exhibiting CLOU behavior, were used. The materials showed different reactivity and oxygen transport capacity depending on their chemical composition, crystallographic phases, and microstructure.

The rank of the studied carriers in methane conversion was Ce–Cu > CeO_2 > Chro. The Ce–Cu carrier was very effective in achieving the full oxidation of methane, whilst CeO_2 allowed either full or partial oxidation. Carbon deposition on CeO_2 was appreciable only for tests carried out at 950 °C. Natural chromite was unsatisfactory because of the absence of any contribution of the prevalent Cr_2O_3 phase.

The study of the process has also shown that the operating conditions and the control of the carrier conversion degree can alternatively lead to the partial (high CO selectivity) or total (high CO_2 selectivity) oxidation of CH_4. Indeed, the selectivity towards carbon monoxide also increases with a longer reduction time. The degree of carrier conversion, tunable by an effective switching strategy between the two cyclic phases of reduction and regeneration, is therefore a key parameter in guiding the process towards the desired products.

The further development of the research will consider steady-state operation, preferably in a circulating fluidized bed where the residence times of the gas and solids in reducing and oxidizing reactors can be easily modified.

Author Contributions: Conceptualization, F.M., F.D. and M.B.; methodology, M.B., A.S. and M.M. (Matteo Minelli); investigation, M.B., A.S. and M.M. (Mauro Mazzocchi); writing—original draft preparation, F.M. and M.M. (Mauro Mazzocchi); writing—review and editing, M.M. (Matteo Minelli) and M.B. All authors have read and agreed to the published version of the manuscript.

Funding: This research was funded under the National Recovery and Resilience Plan (NRRP), Mission 04 Component 2 Investment 1.5—NextGenerationEU, Call for tender n. 3277 dated 30 December 2021 (Award Number: 0001052 dated 23 June 2022).

Data Availability Statement: Data are available upon request to the corresponding author.

Acknowledgments: Valli Granulati srl (I) is acknowledged for the free supply of samples of inert granules used in setting up the experimental equipment.

Conflicts of Interest: The authors declare no conflict of interest.

Nomenclature

Symbols	Meaning	Units
q	Molar flow rate	mmol/min
y_i	Molar fraction of compound i	dimensionless
t	time	Min
m_i	Mass of carrier i	Mg
M_i	Molar mass of compound i	g/mol
e	Equivalence factor for methane oxidation	dimensionless
$n_{O_2\ stoich,\ CH_4}$	Oxygen amount for stoichiometric combustion	mmol
$n_{O_2\ av,carrieri}$	Oxygen availability in carrier	mmol
ξ_{CH_4}	Methane conversion	dimensionless
$\xi_{carrier}$	Conversion of carrier i	dimensionless
η_i	Selectivity for compound i	dimensionless
ω_i	Mass fraction of compound i	dimensionless
Subscripts		
in	Reactor inlet	-
out	Reactor outlet	-
c	Combustion step	-
r	Regeneration step	-

References

1. Abanades, J.C.; Arias, B.; Lyngfelt, A.; Mattisson, T.; Wiley, D.E.; Li, H.; Ho, M.T.; Mangano, E.; Brandani, S. Emerging CO_2 Capture Systems. *Int. J. Greenh. Gas. Control.* **2015**, *40*, 126–166. [CrossRef]
2. Boscherini, M.; Storione, A.; Minelli, M.; Miccio, F.; Doghieri, F. New Perspectives on Catalytic Hydrogen Production by the Reforming, Partial Oxidation and Decomposition of Methane and Biogas. *Energies* **2023**, *16*, 6375. [CrossRef]

3. Lyngfelt, A.; Hedayati, A.; Augustsson, E. Fate of NO and Ammonia in Chemical Looping Combustion—Investigation in a 300 W Chemical Looping Combustion Reactor System. *Energy Fuels* **2022**, *36*, 9628–9647. [CrossRef]
4. Adanez, J.; Abad, A.; Garcia-Labiano, F.; Gayan, P.; de Diego, L.F. Progress in Chemical-Looping Combustion and Reforming Technologies. *Prog. Energy Combust. Sci.* **2012**, *38*, 215–282. [CrossRef]
5. Lu, H.; Shi, X.; Costa, M.; Huang, C. Carcinogenic Effect of Nickel Compounds. *Mol. Cell Biochem.* **2005**, *279*, 45–67. [CrossRef]
6. Otsuka, K.; Sunada, E.; Ushiyama, T.; Yamanaka, I. The Production of Synthesis Gas by the Redox of Cerium Oxide. In *Studies in Surface Science and Catalysis*; Elsevier: Amsterdam, The Netherlands, 1997; pp. 531–536. [CrossRef]
7. Chuayboon, S.; Abanades, S.; Rodat, S. Solar Chemical Looping Reforming of Methane Combined with Isothermal H_2O/CO_2 Splitting Using Ceria Oxygen Carrier for Syngas Production. *J. Energy Chem.* **2020**, *41*, 60–72. [CrossRef]
8. Cheng, Z.; Qin, L.; Fan, J.A.; Fan, L.-S. New Insight into the Development of Oxygen Carrier Materials for Chemical Looping Systems. *Engineering* **2018**, *4*, 343–351. [CrossRef]
9. Warren, K.J.; Scheffe, J.R. Role of Surface Oxygen Vacancy Concentration on the Dissociation of Methane over Nonstoichiometric Ceria. *J. Phys. Chem. C* **2019**, *123*, 13208–13218. [CrossRef]
10. Cheng, Z.; Qin, L.; Guo, M.; Xu, M.; Fan, J.A.; Fan, L.-S. Oxygen Vacancy Promoted Methane Partial Oxidation over Iron Oxide Oxygen Carriers in the Chemical Looping Process. *Phys. Chem. Chem. Phys.* **2016**, *18*, 32418–32428. [CrossRef]
11. Koleli, N.; Demir, A. Chapter 11-Chromite. In *Environmental Materials and Waste. Resource Recovery and Pollution Prevention*; Academic Press: Cambridge, MA, USA, 2016; pp. 245–263. [CrossRef]
12. Nurjaman, F.; Subandrio, S.; Ferdian, D.; Suharno, B. Effect of Basicity on Beneficiated Chromite Sand Smelting Process Using Submerged Arc Furnace. In Proceedings of the International Seminar on Metallurgy and Materials (ISMM2017): Metallurgy and Advanced Material Technology for Sustainable Development, Jakarta, Indonesia, 24–25 October 2017; p. 020009. [CrossRef]
13. Miccio, F.; Ruoppolo, G.; Russo, S.; Urciuolo, M.; De Riccardis, A. Fluidized Bed Combustion of Wet Biomass Fuel (Olive Husks). *Chem. Eng. Trans.* **2014**, *37*, 1–6. [CrossRef]
14. Prasad, R.; Singh, P. A Review on CO Oxidation Over Copper Chromite Catalyst. *Catal. Rev.* **2012**, *54*, 224–279. [CrossRef]
15. Ammendola, P.; Chirone, R.; Lisi, L.; Ruoppolo, G.; Russo, G. Copper Catalysts for H_2 Production via CH_4 Decomposition. *J. Mol. Catal. A Chem.* **2007**, *266*, 31–39. [CrossRef]
16. Warren, K.J.; Carrillo, R.J.; Greek, B.; Hill, C.M.; Scheffe, J.R. Solar Reactor Demonstration of Efficient and Selective Syngas Production via Chemical-Looping Dry Reforming of Methane over Ceria. *Energy Technol.* **2020**, *8*, 2000053. [CrossRef]
17. Storione, A.; Boscherini, M.; Miccio, F.; Landi, E.; Minelli, M.; Doghieri, F. Improvement of Process Conditions for H_2 Production by Chemical Looping Reforming. *Energies* **2024**, *17*, 1544. [CrossRef]
18. Miccio, F.; Natali Murri, A.; Landi, E. Synthesis and Characterization of Geopolymer Oxygen Carriers for Chemical Looping Combustion. *Appl. Energy* **2017**, *194*, 136–147. [CrossRef]
19. Miccio, F.; Landi, E.; Murri, A.N.; Minelli, M.; Doghieri, F.; Storione, A. Fluidized Bed Reforming of Methane by Chemical Looping with Cerium Oxide Oxygen Carriers. *Chem. Eng. Res. Des.* **2023**, *191*, 568–577. [CrossRef]
20. Liu, G.; Lisak, G. Cu-Based Oxygen Carriers for Chemical Looping Processes: Opportunities and Challenges. *Fuel* **2023**, *342*, 127828. [CrossRef]
21. Leion, H.; Lyngfelt, A.; Johansson, M.; Jerndal, E.; Mattisson, T. The Use of Ilmenite as an Oxygen Carrier in Chemical-Looping Combustion. *Chem. Eng. Res. Des.* **2008**, *86*, 1017–1026. [CrossRef]
22. Jing, D.; Arjmand, M.; Mattisson, T.; Rydén, M.; Snijkers, F.; Leion, H.; Lyngfelt, A. Examination of Oxygen Uncoupling Behaviour and Reactivity towards Methane for Manganese Silicate Oxygen Carriers in Chemical-Looping Combustion. *Int. J. Greenh. Gas. Control.* **2014**, *29*, 70–81. [CrossRef]
23. Živković, A.; Sheehama, J.; Warwick, M.E.A.; Jones, D.R.; Mitchel, C.; Likius, D.; Uahengo, V.; Dzade, N.Y.; Meenakshisundaram, S.; Dunnill, C.W.; et al. Structural and Electronic Properties of Cu_4O_3 (Paramelaconite): The Role of Native Impurities. *Pure Appl. Chem.* **2021**, *93*, 1229–1244. [CrossRef]
24. Perrot, P. Chromium–Iron–Oxygen. Ternary Alloy Systems: Phase Diagrams; Crystallographic and Thermodynamic Data. In *Ternary Alloy Systems: Phase Diagrams, Crystallographic and Thermodynamic Data Critically Evaluated by MSIT®*; Springer: Berlin/Heidelberg, Germany, 2009; Volume 11, pp. 250–276. [CrossRef]
25. Jacob, A.; Povoden-Karadeniz, E.; Kozeschnik, E. Revised Thermodynamic Description of the Fe-Cr System Based on an Improved Sublattice Model of the σ Phase. *Calphad* **2018**, *60*, 16–28. [CrossRef]
26. Otsuka, K.; Wang, Y.; Sunada, E.; Yamanaka, I. Direct Partial Oxidation of Methane to Synthesis Gas by Cerium Oxide. *J. Catal.* **1998**, *175*, 152–160. [CrossRef]
27. Fosheim, J.R.; Hathaway, B.J.; Davidson, J.H. High Efficiency Solar Chemical-Looping Methane Reforming with Ceria in a Fixed-Bed Reactor. *Energy* **2019**, *169*, 597–612. [CrossRef]
28. Zhu, M.; Song, Y.; Chen, S.; Li, M.; Zhang, L.; Xiang, W. Chemical Looping Dry Reforming of Methane with Hydrogen Generation on Fe_2O_3/Al_2O_3 Oxygen Carrier. *Chem. Eng. J.* **2019**, *368*, 812–823. [CrossRef]
29. Saddiq, H.A.; Muhammed-Dabo, I.A.; Hamza, A.; Waziri, S.M. Kinetic Modeling of CuO/CeO_2 and CuO/Nb_2O_5 as Oxygen Carriers in the Production of Syngas. *React. Kinet. Mech. Catal.* **2021**, *134*, 727–742. [CrossRef]
30. He, F.; Wei, Y.; Li, H.; Wang, H. Synthesis Gas Generation by Chemical-Looping Reforming Using Ce-Based Oxygen Carriers Modified with Fe, Cu, and Mn Oxides. *Energy Fuels* **2009**, *23*, 2095–2102. [CrossRef]

31. Elgarni, M.M.; Tijani, M.M.; Mahinpey, N. Characterization, Kinetics and Stability Studies of NiO and CuO Supported by Al_2O_3, ZrO_2, CeO_2 and Their Combinations in Chemical Looping Combustion. *Catal. Today* **2022**, *397–399*, 206–219. [CrossRef]
32. Tijani, M.M.; Aqsha, A.; Mahinpey, N. Synthesis and Study of Metal-Based Oxygen Carriers (Cu, Co, Fe, Ni) and Their Interaction with Supported Metal Oxides (Al_2O_3, CeO_2, TiO_2, ZrO_2) in a Chemical Looping Combustion System. *Energy* **2017**, *138*, 873–882. [CrossRef]